Solar-Cycle Warming at the Earth's Surface and an Observational Determination of Climate Sensitivity.

By Ka-Kit Tung and Charles D. Camp

Department of Applied Mathematics, University of Washington, Seattle Washington, USA

ABSTRACT

The total solar irradiance (TSI) has been measured by orbiting satellites since 1978 to vary on an 11-year cycle by about 0.07%. From solar min to solar max, the TSI reaching the earth's surface increases at a rate comparable to the radiative heating due to a 1% per year increase in greenhouse gases, and will probably add, during the next five to six years in the advancing phase of Solar Cycle 24, almost 0.2 °K to the globally-averaged temperature, thus doubling the amount of transient global warming expected from greenhouse warming alone. Deducing the resulting pattern of warming at the earth's surface promises insights into how our climate reacts to known radiative forcing, and yields an independent measure of climate sensitivity based on instrumental records. This model-independent, observationally-obtained climate sensitivity is equivalent to a global double-CO_2 warming of 2.3 -4.1 °K at equilibrium, at 95% confidence level. The problem of solar-cycle response is interesting in its own right, for it is one of the rare natural global phenomena that have not yet been successfully explained.

1. Introduction

Although previously attention has been focused on the UV part of the solar cycle and its absorption by ozone in the stratosphere, the amount of the total solar irradiance (TSI) reaching the earth's surface is not negligible. The observed 0.90 Wm^{-2} variation of the solar constant from solar min to solar max in the last three solar cycles translates into a net radiative heating of the lower troposphere of $\delta Q = \frac{0.90 \bullet 0.85}{4} \sim 0.19$ Wm^{-2}. The factor of 4 is to account for the difference between a unit area on the spherical earth and the circular disk on which the solar constant is measured, while 0.85 is to account for the 15% of the TSI variability that lies in the UV wavelength and is absorbed by ozone in the stratosphere with the remaining reaching the lower troposphere, the surface and the upper ocean [*Lean, et al.*, 2005; *White, et al.*, 1997]. This solar radiative forcing is about 1/20 that for doubling CO_2 ($\delta Q \sim 3.7$ Wm^{-2}). Thus the annual rate of increase in radiative forcing of the lower atmosphere from solar min to solar max happens to be equivalent to that from a 1% per year increase in greenhouse gases, a rate commonly used in greenhouse-gas emission scenarios [*Houghton and et al.*, 2001]. So it is interesting to compare the magnitude and pattern of the observed solar-cycle response to the *transient* warming expected due to increasing greenhouse gases in five years.

The attribution of the observed global warming to the greenhouse-gas increase is difficult because of its non-repeatability, at least not during the period of instrumented records, and of the large uncertainties in the other radiative forcing components (such as black carbon and sulphate aerosols [*Hansen, et al.*, 2005]). Consequently General Circulation

Models (GCM) are indispensable both in explaining the warming that has occurred and in predicting the future climate if the greenhouse gases continue to increase. Confidence in these models would be greatly increased if their climate sensitivity---currently with a factor of three uncertainty, yielding 1.5 °K to 4.5 °K equilibrium warming (ΔT_{2xCO2}) due to a doubling of CO_2 in the atmosphere [*Houghton and et al.*, 2001]---can be calibrated against nature's. On the other hand there is a recurrent warming of the earth by the solar cycle. The periodic nature of the phenomenon allows the use of more sophisticated signal processing methods to establish the reality of the signal. Since the forcing is known, contrasting solar-max and solar-min years over multiple periods yields a pattern of earth's *forced* response, which is better than previous attempts of using "warm-year analogs in recent century"--- some of which may be due to unforced variability --- to infer information relevant to future CO_2 forcing. Our procedure for the solar-cycle signal yields an interesting pattern of warming over the globe. It may be suggestive of some common fast feedback mechanisms that amplify the initial radiative forcing. Currently no GCM has succeeded in simulating a solar-cycle response of the observed amplitude near the surface. Clearly a correct simulation of a global-scale warming on decadal time scale is needed before predictions into the future on multi-decadal scale can be accepted with confidence.

There have been thousands of reports over two hundred years of regional climate responses to the 11-year variations of solar radiation, ranging from cycles of Nile River flows, African droughts, to temperature measurements at various selected stations, but a coherent global signal at the surface has not yet been established statistically [*Hoyt and Schatten*, 1997; *Pittock*, 1978]. Since the forcing is global, theoretically one should expect a global-scale response. When globally and annually averaged and detrended, but otherwise unprocessed, the surface air temperature since 1959 (when modern rawinsonde network was established) is seen in Figure 1 (reproduced from *Camp and Tung* [2007c]) to have an interannual variation of about 0.2 °K, somewhat positively correlated with the solar cycle, although the signal also contains a higher-frequency variation of comparable magnitude, possibly due to El Niño-Southern Oscillation (ENSO).

To filter out the non-decadal variability, we consider an approach which turns out to be very effective: that is to take advantage of the spatial characteristics of the solar-cycle response. One rudimentary way to obtain the spatial pattern objectively is to use the difference between the solar-max composite and the solar-min composite. This Composite Mean Difference (CMD) Projection method has been discussed in *Camp and Tung* [2007c]. Projecting the original detrended, annual-mean data onto this spatial pattern yields a time series with the higher- frequency variability filtered out, yielding a higher correlation coefficient of ρ=0.64, and higher amplitude of κ=0.18±0.08 °K per Wm^{-2}. We can do even better in reducing the error bar, using a more sophisticated optimization method described below.

2. Spatial-time filter

Early estimates of the solar-cycle response were obtained using *model-generated* “optimal space-time filter”[*Stevens and North*, 1996] , whose pattern is small over the poles as compared to the tropics. This may be a reason for the very small global-mean surface temperature obtained, about 0.06 K; the pattern obtained *objectively* from data is very different (see Figure 2a). We use here the method of Linear Discriminant Analysis

(LDA) developed by *Schneider and Held* [2001] originally to deduce the temperature trends, and later by *Camp and Tung* [2007a; 2007b] for studying the QBO, solar cycle and ENSO perturbations; more detail on the implementation of the method for the present problem, including mathematical formulae, can be found in the latter references. Although less intuitive than the CMD Projection method, the LDA method is necessary here to reduce the error bars of the response for the purpose of using it to deduce the range of climate sensitivity; the results obtained by the CMD method of Camp and Tung (2007a) have an error bar which is just a little too large to be useful. The input information used to construct the "solar-cycle filter" is rather minimal and objective: it simply specifies what years are in the solar-max group and what years belong to the solar-min group. The LDA procedure, which maximizes the ratio *R* of the between-group variance relative to the variance within each group, then produces the latitudinal weights from which we obtain both the filtered time series and the associated spatial pattern that best distinguish the solar-max group from the solar-min group by filtering out other atmospheric variability, such as ENSO. Previously used methods, multiple regressions and composite differences, have not been able to establish a statistically-significant coherent global pattern; these methods do not take advantage of the spatial information of the response. There is a subtle but important difference in the LDA approach used here as compared to methods that project the data onto a spatial pattern, including the EOF projection and the CMD projection [*Camp and Tung*, 2007c]: Using the present solar-cycle signal problem as an example, the residual's spatial pattern obtained by the projection methods is orthogonal to the retained pattern, but can still contain in its time domain decadal (viz. 11-year period) signal. The residual in the LDA method, on the other hand, contains no decadal signal; all such signals have optimally been included in the retained mode.

Figure 2a shows the meridional pattern thus obtained for the zonal-mean, annual-mean air temperature at the surface using the global dataset of NCEP [*Kalnay, et al.*, 1996], linearly detrended to remove the secular global-warming signal. Figure 3a shows the corresponding temperature pattern in the 850-500 hPa layer, representing the lower troposphere. The amplitude of the warming is about 24% larger in the atmospheric layer above the surface. The surface pattern in Figure 2 shows clearly the polar amplification of warming, predicted by models for the global warming problem, with largest warming in the Arctic (3 times that of the global mean), followed by that of the Antarctic (2 times). Surprisingly this warming occurs during late winter and spring (not shown) over the polar region. Since the tropical atmosphere is more opaque, a warmed surface cannot re-radiate all the energy it receives back to space. The excess radiative energy must be transported by dynamic heat fluxes to the high latitudes, resulting in polar warming [*Cai*, 2005; , 2006; *Cai and Lu*, 2006]. This occurs rather quickly, in 5 years or less, and probably involves mostly the atmosphere and the upper oceans, as *White et al.* [1997] showed that the solar-cycle response does not penetrate deep enough into the ocean to engage the deep water. Low warming occurs over the latitudes of the Southern ocean and over the Southern tropics. In general, warming over the oceans is much less than over land (see later). Over the tropics, not much warming occurs whether it is over land or over ocean. The warming over the tropics instead occurs higher up, at 200 hPa (not shown, at only 90% confidence level because of the quality of the upper air data prior to 1979), which is where the latent heat due to vertical convection is deposited. *Cai* [2005] discusses how the vertical transport of surface heating in a moist atmosphere leads to an increase in poleward heat transport despite the weakening of the surface-temperature gradient.

Many of the general features are similar to those predicted for global warming [*Manabe and Stouffer*, 1980]. Using a bootstrap Monte-Carlo test with replacement in Figures 2b and 3b, we show that a single optimal filter exists that separates the solar-max years from the solar-min years in temperature and that the large observed separability measure *R* could not have been obtained by chance at over 95% confidence level.

Volcanic eruptions, particularly El Chichón in March 1982 and Pinatubo in June 1991, coincidentally occurring during solar maxes, may contaminate the 11-year signal. The expected cooling in the troposphere for the transient aerosol events however lasted temporarily, for about two to three years. Since the LDA analysis does not require a continuous time series, the volcano-aerosol years can be excluded from the time series and a new discriminant pattern generated. This has been done in Figures 2 and 3, where the years 1982 and 1983 (after El Chichón), and 1992 and 1993 (after Pinatubo) are excluded. Removing a third year, or removing only one year, does not change the results. When no volcanic years were excluded in the LDA analysis, the warming amplitude is still the same but the confidence level is 4-5% lower (not shown).

The projection of the annual means of years from 1959 to 2004 onto the discriminant spatial weights is shown in Figure 2c and 3c. Given that our method requires only the data be divided into two groups with no information on the peak amplitudes of either the solar irradiation or the temperature response, it is remarkable that the deduced global-temperature response follows the solar-radiation variability so well. The correlation coefficient is ρ=0.84 and 0.85 in Figure 2 and 3, respectively, and is highly statistically significant. This establishes that the surface (and lower tropospheric) temperature response is related to the solar-cycle forcing at over 95% confidence level. Such an attribution of response to forcing has not been statistically established for the greenhouse global-warming problem. Our result shows a global-mean warming of almost 0.2°K at the surface (0.3° K in the layer above) from solar min to solar max in the last three cycles. More precisely, we fit $\delta T = \kappa\ \delta S$ to all 4.5 solar cycles, where $\delta S(t)$ is the TSI variability time series, and find κ=0.167± 0.037 °K/(Wm^{-2}) at the surface (and 0.213±0.044 in 500-850 hPa). The error bars define a 95% confidence interval and are approximately equal to ±2 standard deviations (σ). This value of κ is about 50-70% (a factor of 2) higher than the regression coefficients of temperature against irradiance variability previously deduced [*Douglass and Clader*, 2001; *Lean*, 2005; *Scafetta and West*, 2005], of ~0.1 ^{o}K global-mean surface warming attributable to the solar cycles. Our higher response level is however consistent with some other recent reports [*Haigh*, 2003; *Labitzke, et al.*, 2002; *Van Loon, et al.*, 2004], and with the earlier finding of *Coughlin and Tung* [2004] using a completely different method in the time domain, who also found the zonal-mean warming to be positively correlated with the solar-cycle index over most of the troposphere.

3. Error analysis

The error bar in κ shown above is due only to regression error. To see if there are other possible errors that give a larger error bar, we perform the so-called *N-1* error analysis, in which we sequentially drop each year and perform a new LDA analysis until all possibilities are covered. This leads to $\kappa=0.167\pm0.014$ at the surface (and 0.213 ± 0.020 in 500-850 hPa). The 2σ error bar is much smaller than the regression error, showing that the amplitude of κ is not affected by any one anomalous data point. Dropping *m* data points, if they are independent, increases the error bar relative to dropping one point by a factor of $m^{1/2}$. Monte-Carlo simulations show that this is approximately true even without the independence-assumption, for *m* not too large. The error bars from the *N-m* test would still be less than the regression error unless more than 20% of the data are in error and dropped, which is highly unlikely. Thus, we obtain the following overall bounds for κ: $\kappa=0.17\pm0.04$ °K/(Wm^{-2}) for the surface air-temperature response to variations in the solar constant.

In NCEP reanalysis, temperature product is influenced by the model used in the reanalysis at the surface more than at constant pressure surfaces. We repeated the LDA analysis on the 925 hPa NCEP temperature, a “type A” product not much affected by model reanalysis, and obtained the same $\kappa=0.17\pm0.04$ °K/(Wm^{-2}), at 100% confidence level. Instrumental errors are not included in our error bars. Because satellite measurement was not available until after 1978, our use of reconstructed TSI for the period 1959-1978 presents another source of error. An upper bound on this error is obtained by redoing the LDA dropping all years prior to 1979. We find that κ is reduced by 3%, a magnitude of difference well below the stated error bar. Note that the contamination of the signal by other variability, such as volcanoes and ENSO, has been minimized by our method. The greenhouse-warming signal is removed to the extent possible by the linear trend. However, the linear trend may be sensitive to the end point and unfortunately 2005 is a very unusual year (one of the warmest on record). To minimize this end-point error, only 1959-2004 were used in the analysis. To include 2005, a nonlinear trend may need to be used.

4. Detailed spatial pattern

Having established the existence of a global-scale solar-cycle response we can also examine in more detail the surface-warming pattern over the globe. We repeat the LDA analysis on the gridded NCEP surface air-temperature data at a latitude-longitude resolution of $5^o x 5^o$. Consistent with the zonal-mean pattern shown in Figure 2, the largest warming in Figure 4 occurs over the two polar regions. Polar projections can be found in Figure 5. Warming of close to 1°K occurs near seasonal sea-ice edges in the Arctic Ocean and, to a smaller extent, around the Antarctic continent on the seaward side, strongly suggestive of a positive sea-ice-albedo feedback as a mechanism for the polar amplification of the radiative forcing. Although the whole of the western Arctic is warm, largest warming occurs around the "Northwest Passage" (the Canadian Archipelago, Beaufort Sea, the coast of northern Alaska and the Chukchi Sea between Alaska and Siberia). The warm pattern is quite similar to the observed recent trend [*Moritz, et al.*, 2002], and may suggest a common mechanism. In the midlatitudes, there is more warming over the continents than over the oceans. Most of Europe is warmed by 0.5 °K, and eastern Canada by 0.7 °K, while western U.S. sees a smaller warming of 0.4-0.5 °K.

Iraq, Iran and Pakistan are warmer by 0.7 °K and Northern Africa by 0.5 °K. Curiously the Andes in the South America continent is colder by 0.7 °K.

To ascertain the robustness of these patterns to whether the end of the time series occurs during a solar max or a solar min, the time series is truncated after the maximum of the last solar cycle in 2003 and again after the solar min of 1997, and the LDA repeated. The patterns in Figure 3 remain unchanged except that the Arctic warming gradually loses its detail with shorter and shorter records and becomes defused over the whole western half of the Arctic.

5. Explaining the solar-cycle response

In the absence of fast feedbacks, the tropospheric heating of $\delta Q \sim 0.19$ Wm^{-2} from solar min to solar max is balanced by infrared reemission and it would have produced at the surface a temperature change of $\delta T \sim \delta Q\ (1-\alpha)/B \sim 0.07$ °K, taking into account that a fraction $\alpha = 0.30$ is reflected back to space. The increase in infrared reemission is given by $B\delta T$ with $B = 1.9$ Wm^{-2} per °K [*Graves, et al.*, 1993]. Our observed global-mean warming of ~0.2 °K would seem to imply that, if it is due to TSI heating at the surface, the fast feedback processes in our atmosphere, such as ice-albedo, lapse-rate, water-vapor and cloud feedbacks, should in aggregate amplify the initial TSI warming by about a factor of $f \sim 2$- 3. (This factor should be larger than 2 because the phenomenon is periodic and not at equilibrium; see Appendix *Analysis*.) From the large body of work on radiative-feedback processes related to the global-warming problem [*Bony, et al.*, 2006], we know that a “climate-amplification factor” of this range is justifiable physically. Because of the fast timescales involved in these processes, it is reasonable to expect that the same feedback factor applies to the decadal phenomenon as well. Previous GCM calculations [*Haigh*, 1996; *Shindell, et al.*, 1999] have tended to underestimate the response to solar cycle forcing possibly because, as pointed out by *Haigh* [1996], the fixed sea-surface temperature in these models might have reduced the surface heating and the magnitude of the feedback processes.

In the troposphere the phenomena of solar cycle and global warming are quite similar. The radiative forcing for both is global in extent and relatively uniform, although solar forcing occurs only where the sun shines. (Our use of annual means aims at reducing this difference.) The main difference lies in the stratosphere, but the effect of these differences on the near surface temperature is expected to be small. The stratosphere in solar max warms due to ozone absorption of the UV portion of the solar-constant variation, which, with a variability of 0.12 Wm^{-2} [*Lean, et al.*, 2005], is larger, in percentage terms, than the variability in the TSI. The effect of the solar-cycle ozone warming in the tropical stratosphere, which is about 0.5-1.5 °K, on the lower troposphere has been investigated by GCMs [*Haigh*, 1999; *Shindell, et al.*, 1999] and is found to be small: Haigh [1996]found that the Hadley circulation is shifted slightly, by 0.7 ^{o} of latitude. There is evidence in our Figure 3a of the two midlatitude strips of warming suggested by her as a result of this shift, but this feature does not extend to the surface. *Shindell et al.* [1999] found that on a global-mean basis, the net surface warms by about 0.07 °K, including both the stratospheric influence and direct heating of the surface (but with fixed sea surface temperature). The observed solar cycle related heating over the polar stratosphere is larger, at 7 °K [*Camp and Tung*, 2007a], but this occurs only during late winter and over a small area, related to the enhanced frequency of occurrence of the Stratospheric Sudden Warming phenomenon [*Labitzke*, 1982]. Although the effect can be transmitted to the polar troposphere [*Baldwin and Dunkerton*, 1999] , the anomaly near the surface on a global and annual mean is small. If these stratospheric differences can be ignored, the surface warming seen in Figure 2 in the zonal mean, and in more detail in Figure 4, may give a hint of the initial transient greenhouse warming at the surface in 5-6 years. This is because at a projected 1% increase per year of the greenhouse gases it takes about five years to increase the radiative forcing to the 0.19 Wm^{-2} in δQ responsible for the response shown in these figures. Longer than a few decades, response to a monotonically increasing forcing in the greenhouse-gas problem engages the deep water, and the two problems cannot be scaled.

6. Model-independent determination of climate sensitivity

Considerable progress has been made since the last three IPCC reports in reducing the range of model sensitivity with better understanding of the physical processes involved in the feedback mechanisms [*Bony, et al.*, 2006], and these efforts have helped narrow the range of model-to-model difference . Within a single model, a 5-95% probable range of climate sensitivity can be established by varying model parameters. For example *Murphy et al.* [2004] obtained the range 2.4-5.4 °K for ΔT_{2xCO2} for the HadAM3 model, but pointed out that this should be recognized as a lower bound of the range because it may change with changing resolution for the same model and with changing to a different model. The latest version of NCAR's Community GCM, CCSM3, has a sensitivity of 2.32 °K for its low resolution and 2.71 °K for its highest resolution version [*Kiehl, et al.*, 2006]. As this model evolved from version CCSM1.4 to CCSM3, its sensitivity changed from 2.01 to 2.27 to 2.47 °K.

Truly model-independent determination of climate sensitivity has been rare. A measure of climate sensitivity not restricted to the CO_2 problem can be defined as the ratio of the global-temperature response to the radiative forcing change, $\lambda=\delta T/\delta Q$. This quantity is expected to be different for different time scales. The equilibrium climate sensitivity is commonly used in inter-model comparisons. Paleo-climate data over thousands of years can be assumed to be in equilibrium and the equilibrium climate sensitivity deduced. Vostok ice core drillings have yielded past proxy surface temperature from deuterium isotope fractionation and greenhouse-gas concentration from gases trapped in the ice sample. Although these can be used to yield a global concentration of greenhouse gases because they are well mixed, global-mean temperature cannot be determined from a local polar region. Using a GCM *Hansen et al.* [1993] calculated a global cooling of 3.7 °K compared to present by specifying the CLIMAP reconstructed boundary conditions and estimated radiative forcing of 7.1 ±2.0 Wm^{-2} during the last major ice age of 18,000 years ago. Taken at face value these would have yielded a low climate sensitivity of λ_{eq}~0.52±0.15 °K per Wm^{-2}. The authors however thought the CLIMAP reconstruction may be inconsistent with some land proxy in the tropics of 3 to 5 °K cooling, and chose a "best estimate" of 5 °K as the global ice-age cooling. This then led to the oft-quoted estimate of climate sensitivity of ~0.75±0.25 °K per Wm^{-2}, implying $\Delta T_{2xCO2}=\lambda_{eq}\delta Q$~2.8±0.9 °K [*Hansen, et al.*, 2005; *Lorius, et al.*, 1990], consistent with the GISS GCM. Obviously the stated error bars should have been much larger. In an attempt to derive a model-independent climate sensitivity, *Hoffert and Covey* [1992] obtained an estimate of global mean cooling of -3.0±0.6 °K using CLIMAP tropical ocean temperature reconstruction during the Last Glacial Maximum by assuming that there is a universal latitudinal profile of temperature change. This allowed the authors to convert regional cooling proxy to global mean, and derive a lower climate sensitivity of 2.0±0.5 °K. The assumption of unchanging temperature gradient as our climate warms or cools is questionable and, even if approximately true, should have a large error bar. *Shaviv* [2005] averaged the tropical ocean- and land- proxy temperatures but increased the error bars to obtain $\lambda_{eq} \sim 0.58^{+0.29}_{-0.20}$ °K per Wm^{-2}. This yielded a rather low lower bound of 1.0 °K warming for ΔT_{2xCO2}. *Shaviv* [2005] further estimated that the climate sensitivity could be even lower by 20% if the effect of cosmic-ray flux, assuming it induces low-altitude clouds cover in the tropics, is included, but this effect, which is itself uncertain, is smaller than the error bar. Recently *Hegerl et al.* [2006] used 700 years of reconstructed temperature data and showed that a simple energy-balance model can best produce the observed climate variation if the model climate sensitivity ΔT_{2xCO2} is 1.5-6.2 °K. This estimate is model-dependent. It also depends on the uncertain reconstruction of radiative forcing and its variation during the 700 years. Similarly *Wigley and Raper* [2002] found that the historical record can be simulated if the energy-balance model has a climate sensitivity of 3.4 °K. The surface cooling after the Pinatubo volcanic eruption has been used, with the help of a GCM, to constrain the magnitude of the water-vapor feedback process (as giving rise to a magnification of climate response by 60%) [*Soden, et al.*, 2002].

Model-independent estimates of climate sensitivity were obtained by *Forster and Gregory* [2006] using 11 years of Earth Radiation Budget data (1985-1996) and a novel analysis of the net radiative imbalance *F* at the top of the atmosphere. The net imbalance is the difference between the shortwave radiative heating *Q* and longwave cooling. By regressing *F-Q* against global surface temperature *T*, the authors obtained the slope λ^{-1}~ 2.3±1.4 Wm^{-2} per °K, from which they deduced ΔT_{2xCO2} ~ 1.0-4.1 °K for the 95% confidence interval, on the implicit assumption of uniform priors in the λ^{-1} space [*Frame, et al.*, 2005]. The lower bound of 1.0 °K is too low to rule out the possibility of negative feedback, but we hope to combine our result with this to arrive at a narrower bound. *Gregory at al.* [2002], using observational estimates of the increase in ocean heat uptake from 1957 to 1994, which is responsible for the imbalance *F,* and an estimate of *Q*, found 1.6 °K< ΔT_{2xCO2}< ∞.

Using the globally-averaged solar-cycle response, which is directly measured, we can obtain λ for the decadal time scale in the following way. The regression coefficient κ is related to λ as:

$$\lambda=\delta T/\delta Q=\kappa\delta S\ /\delta Q=0.80\pm0.19\ °K\ per\ watt\ m^{-2}<\lambda_{eq} \qquad (1)$$

using $\delta Q=\ \delta S 0.85/4$. This corresponds to a global warming of 3.0 ±0.7 °K for δQ =3.7 Wm^{-2}. The last inequality in (1) is obtained because periodic response is lower than equilibrium response: If the same δQ is maintained for two centuries instead of being reversed every 5.5 years, the warming should have been larger. Nevertheless, since the observed time lag in the solar-cycle response is small (see *Appendix*), our best guess is that the equilibrium climate sensitivity should not be too different from 3.0 °K.

It should be noted that unlike the lower bound given above, an estimate of the upper bound is model-dependent and thus less certain (see Appendix *Analysis*). It is commonly known that using a transient phenomenon to deduce equilibrium climate sensitivity can lead to a large error bar [*Houghton and et al.*, 2001], but the uncertainty is biased towards the upper bound. Nevertheless no *useful* lower bound can be obtained if the frequency of the transient phenomenon is too high. Fortunately, a period of 11years is long enough to yield a useful lower bound. We can combine our lower bound, obtained completely independent of models, with the upper bound obtained also in a model-independent way by *Forster and Gregory* [2006] (subject to the assumption of priors mentioned above) to yield the following 95% confidence interval:

$$2.3\ °K < \Delta T_{2xCO2} < 4.1\ °K\ . \quad (2)$$

The lower bound of 2.3 °K happens to be the same as the model-derived value (2.4 °K) of *Murphy et al* [2004] after converting it into the 5-95% range of the latter; it is ~1 °K higher than the previous IPCC lower bound.

This observationally-determined climate-sensitivity range likely rules out the case of no positive feedback (ΔT_{2xCO2}<1.4 °K). It suggests models with lower equilibrium sensitivity, such as NCAR's CSM1 (with ΔT_{2xCO2}~2.0 °K), and DOE's PCM (< 2.0 °K) [*Houghton and et al.*, 2001] as very unlikely to be consistent, and that models with medium sensitivity, such as GISS's ModelE (2.7 °K), NCAR's high-resolution version of CSM3 (2.7 °K), Hadley Center's HadGem1 (2.8 °K) and GFDL's CM2.0 (2.9 °K) are very likely to be consistent with the deduced lower bound. Furthermore, unlike that deduced from conditions of last glacial maximum, when the surface conditions and albedo were very different than those in the current climate, the values in (2) may be closer to that in the world of doubled CO_2.

7. Conclusion

Using NCEP reanalysis data that span four and a half solar cycles, we have obtained the spatial pattern over the globe which best separates the solar-max years from the solar-min years, and established that this coherent global pattern is statistically significant using a Monte-Carlo test. The pattern shows a global warming of the Earth's surface of about 0.2 °K, with larger warming over the polar regions than over the tropics, and larger over continents than over the oceans. It is also established that the global warming of the surface is related to the 11-year solar cycle, in particular to its TSI, at over 95% confidence level. Since the solar-forcing variability has been measured by satellites, we therefore now know both the forcing and the response (assuming cause and effect). This information is then used to deduce the climate sensitivity. Since the equilibrium response should be larger than the periodic response measured, the periodic solar-cycle response measurements yields a lower bound on the equilibrium climate sensitivity that is equivalent to a global warming of 2.3 °K at doubled CO_2. A 95% confidence interval is estimated to be 2.3-4.1 °K. This range is established independent of models.

Acknowledgements

The research is supported by grant ATM-3 32364 from National Science Foundation, Climate Dynamics Program. We thank Professor Brian Farrell for encouraging us to pursue the climate sensitivity problem using our solar cycle result. We thank Dr. Judith Lean for providing us with her reconstructed TSI and UV time series.

References

Baldwin, M. P., and T. J. Dunkerton (1999), Propagation of the Arctic Oscillation from the stratosphere to the troposphere, *J. Geophys. Res.-Atmos.*, *104*, 30937-30946.

Bony, S., et al. (2006), How well do we understand and evaluate climate change feedback processes, *J. Climate.*, *19*, 3445-3482.

Cai, M. (2005), Dynamical amplification of polar warming, *Geophys. Research. Lett.*, *32*, L22710,doi:22710.21029/22005GL024481.

Cai, M. (2006), Dynamical greenhouse-plus feedback and polar warming amplification. Part I: A dry radiative-transportive climate model, *Clim. Dyn.*, DOI 10.1007/s00382-00005-00104-00386.

Cai, M., and J. Lu (2006), Dynamical Greenhouse-plus feedback and polar warming amplification. Part II: meridional and vertical asymmetries of the global warming, *Clim. Dyn.*, *submitted*.

Camp, C. D., and K. K. Tung (2007a), The influence of the solar cycle and QBO on the late winter stratospheric polar vortex, *J. Atmos. Sci.*, *64*, 1267-1283.

Camp, C. D., and K. K. Tung (2007b), Stratospheric polar warming by ENSO in winter: A statistical study, *Geophys. Research. Lett.*, *34*, L04809, doi:04810.01029/02006GL028521.

Camp, C. D., and K. K. Tung (2007c), Surface Warming by the Solar Cycle as Revealed by Composite Mean Difference Projection, *Geophys. Research. Lett.*, *submitted*.

Coughlin, K., and K. K. Tung (2004), Eleven-year solar cycle signal throughout the lower atmosphere, *J. of Geophy. Res.-Atmospheres*, *109*.

Douglass, D. H., and B. D. Clader (2001), Climate sensitivity of the Earth to solar irradiance, *Geophys. Research. Lett.*, *16*, doi:10.1029/2002GL015345

Forster, P. M., and J. M. Gregory (2006), The climate sensitivity and its components diagnosted from Earth Radiation Budget data, *J. Climate.*, *10*, 39-52.

Frame, D. J., et al. (2005), Constraining climate forecasts: the role of prior assumptions, *Geophys. Research. Lett.*, *32*, doi:10.1029/2004GL022241.

Graves, C. E., et al. (1993), New Parameterizations and Sensitivities for Simple Climate Models, *J. Geophys. Res.-Atmos.*, *98*, 5025-5036.

Gregory, J. M., et al. (2002), An observationally based estimate of the climate sensitivity, *J. Climate.*, *22*, 3117-3121.

Haigh, J. D. (1996), The impact of solar variability on climate, *Science*, *272*, 981-984.

Haigh, J. D. (1999), A GCM study of climate change in response to the 11-year solar cycle, *Q. J. R. Meteor. Soc.*, *125*, 871-892.

Haigh, J. D. (2003), The effects of solar variability on the Earth's climate, *Philos. Trans. R. Soc. Lond. Ser. A-Math. Phys. Eng. Sci.*, *361*, 95-111.

Hansen, J., et al. (1993), How sensitive is the world's climate?, *National Geographic Research & Exploration*, *9*, 142-158.

Hansen, J., et al. (2005), Earth's Energy Imbalance: Confirmation and Implications, *Science*, *308*, 1431-1435.

Hegerl, G. C., et al. (2006), Climate sensitivity constrained by temperature reconstructions over the past seven centuries, *Nature*, *440*, 1029-1032.

Hoffert, M. I., and C. Covey (1992), Deriving global climate sensitivity from palaeoclimate reconstructions, *Nature*, *360*, 573-575.
Houghton, J. T., and et al. (2001), *Climate Change 2001, The Scientific Basis*, Cambridge University Press, Cambridge.
Hoyt, D. V., and K. H. Schatten (1997), *The role of the sun in climate change*, 279 pp., Oxford University Press, New York.
Kalnay, E., et al. (1996), The NCEP/NCAR 40-year reanalysis project, *Bull. Amer. Meteorol. Soc.*, *77*, 437-471.
Kiehl, J. T., et al. (2006), The climate sensitivity of the Community Climate System Model Version 3 (CCSM3), *J. Climate.*, *19*, 2584-2596.
Labitzke, K. (1982), On the Interannual Variability of the Middle Stratosphere During the Northern Winters, *J. Meteorol. Soc. Jpn.*, *60*, 124-139.
Labitzke, K., et al. (2002), The global signal of the 11-year solar cycle in the stratosphere: observations and models, *J. Atmos. Sol.-Terr. Phys.*, *64*, 203-210.
Lean, J. (2005), Living with a variable sun, *Phys. Today*, *58*, 32-38.
Lean, J., et al. (1995), Reconstruction of Solar Irradiance since 1610 - Implications for Climate-Change, *Geophysical Research Letters*, *22*, 3195-3198.
Lean, J., et al. (2005), SORCE contributions to new understanding of global change and solar variability, *Sol. Phys.*, *230*, 27-53.
Lorius, C., et al. (1990), the ice-core record: climate sensitivity and future greenhouse warming, *Nature*, *347*, 139-145.
Manabe, S., and R. J. Stouffer (1980), *J. Geophys. Res.*, *85*, 5529.
Moritz, R. E., et al. (2002), Dynamics of recent climate change in the Arctic, *Science*, *297*, 1497-1502.
Murphy, J. M., et al. (2004), Quantification of modelling uncertainties in a large ensemble of climate change simulations, *Nature*, *430*, 768-772.
Pittock, A. B. (1978), A critical look at long-term sun-weather relationships, *Reviews of Geophysics and Space Physics*, *16*, 400-420.
Scafetta, N., and B. J. West (2005), Estimateed solar contribution in the global mean surface warming using ACRIM TSI satellite composite, *Geophys. Research. Lett.*, *32*, doi:10.1029/2005GL023849.
Shaviv, N. J. (2005), On climate response to changes in the cosmic ray flux and radiative budget, *J. Geophys. Res.*, *110*, doi:10.1029/2004JA010866.
Shindell, D., et al. (1999), Solar cycle variability, ozone, and climate, *Science*, *284*, 305-308.
Soden, B. J., et al. (2002), Global cooling after the eruption of Mount Pinatubo: A test of climate feedback by water vapor, *Science*, *296*, 727-730.
Stevens, M. J., and G. R. North (1996), Detection of the climate response to the solar cycle, *Journal of Atmospheric Sciences*, *53*, 2594-2608.
Van Loon, H., et al. (2004), A decadal solar effect in the tropics in July-August, *J. Atmos. Solar-Terr. Phys.*, *66*, 1767-1778.
White, W. B., et al. (1997), Response of global upper ocean temperature to changing solar irradiance, *J. Geophys. Res.-Oceans*, *102*, 3255-3266.
Wigley, T. M. L., and S. C. B. Raper (2002), Implications for climate and se level of revised IPCC emissions scenarios, *Nature*, *357*, 293-300.

Appendix

Analysis: Energy balance at the surface:

The purpose of this section is to show that the observed solar cycle response is energetically consistent with the magnitude of the forcing and typical and reasonable values of ocean heat flux and atmospheric feedback amplifications. It is not meant to be a model calculation of the solar-cycle response.

Consider the heat budget of atmosphere near the surface, where *T(y,t)* is the surface temperature:

$$C\frac{\partial}{\partial t}\overline{T} = Q(1-\overline{\alpha}) - (A + B\overline{T}) + \frac{\partial}{\partial z}\overline{F_z}, \qquad (3)$$

where the overhead bar denotes global averaging. Eq.(3) states that the heat content of the atmosphere is increased by radiative forcing (first term on the right) and by heat flux to the oceans below (the last term), and decreased by infrared emission to space above (second term). The global average removes the meridional dynamical transport of heat term, since the latter is usually written in the form of a divergence. However, the presence of poleward heat transport and polar amplification of warming can increase the global mean warming by 10% [*Cai*, 2005]. This is ignored here in our discussion of global climate sensitivity. Q is ¼ of the solar constant, and $\alpha(y)$ is the albedo-- the fraction of the sun's radiation reflected back to space by clouds and surface. $(A+BT)$ is the linearized form of the infrared emission of the earth to space fitted from observational data on outgoing long-wave radiation, with A=202 Wm^{-2}, and B=1.90 Wm^{-2} °K^{-1} in the current climate. They are temperature dependent if the current climate is perturbed. The parameter C in Eq. (3) represents the thermal capacity of the atmosphere. We write τ=C/B, which measures the time scale due to the climate system's inertia. $\overline{\alpha}$ is the weighted global average albedo. The overbar is henceforth dropped for convenience. Considering small radiative perturbation δQ in $Q=Q_0+\delta Q$, the equation governing the small temperature perturbation can be obtained from the first variation of the above equation, with B and α expanded in a Taylor series in T. This leads to the following perturbation equation:

$$
\begin{aligned}
&B\tau\frac{\partial}{\partial t}\delta T=(1-\alpha)\delta Q-B\delta T/f+\frac{\partial}{\partial z}\delta F_z,\\
&where\\
&f=1/(1-g),\\
&g=(-\frac{T}{B}\frac{\partial}{\partial T}B-\frac{Q}{B}\frac{\partial}{\partial T}\alpha)_0
\end{aligned}
\tag{4}
$$

The factor f is the controversial climate gain, and g is the effect of temperature dependent feedback factors, include the water-vapor feedback (in the first term) and, ice- and snow-albedo feedback (in the second term). Cloud feedback has contributions in both terms. For solar-cycle response, we model the flux to the ocean as diffusive (i.e. $F_z=-CD\partial T/\partial \mathrm{z}$) with an exponential decay scale in the upper ocean as if it is semi-infinite (and so $\partial(\delta T)/\partial \mathrm{z}=-\mu\delta T$). This is equivalent to neglecting the main thermocline; this is appropriate for the solar-cycle response, which does not penetrate deep enough into the ocean. Thus the last term in (4) becomes $-CD\mu^2\ \delta T$.

Periodic solution:

$$
\begin{aligned}
&If: \delta Q = a\cos(\omega t),\\
&then: \delta T = \frac{(1-\alpha)\delta Q(t-\Delta)\tilde{f}}{B}\frac{1}{\sqrt{1+\varepsilon^2}},\\
&where: \varepsilon = \tilde{f}\omega\tau; \omega\Delta = \tan^{-1}(\varepsilon); \tilde{f} \equiv \frac{f}{1+D\mu^2 f\tau}.
\end{aligned}
\qquad (5)
$$

Compared to the steady-state solution for a steady forcing, the periodic solution is delayed by the phase lag of Δ, and its amplitude is diminished by the factor $(1+\varepsilon^2)^{-1/2}$. Since the phase lag and the amplitude factor are related, an observation of the phase lag of the solar cycle also gives an estimate of the amplitude ratio between the periodic solution and the equilibrium solution.

For an oscillating heating which reverses every 5.5 years, we do not expect the solar-cycle heating to penetrate too deeply into the ocean. *White et al.* [1997] found that the solar- cycle signal penetrated only $1/\mu$~100m into the upper ocean, with no effect from the deep water below the main thermocline, and that the observed phase lag in the ocean response peaked at 1-2 years. Atmospheric lag should be shorter than the lag in the ocean response. In fact the correlation coefficient ρ between the atmospheric temperature projection and the solar flux peaks at zero phase-lag and drops precipitously for larger lags, except possibly for a lag or lead of 1 year (separate LDA analysis with shifted time series not shown). For an explanation of the global-mean solar-cycle signal we take typical values of D~1.0 cm^2/s, and f~2.6. Eq. (5) then yields:

$\lambda = \frac{\delta T}{\delta Q} = \frac{(1-\alpha)\tilde{f}}{B\sqrt{1+\varepsilon^2}}$ ~0.61 °K/(watts m^{-2}) for a lag of Δ~+-1 year, and ~0.96 °K/(Wm^{-2}) for no phase lag. Both are within the range of the observed response (1). Thus we consider the global surface response to the 11-year solar cycle explainable primarily by

TSI forcing magnified by a factor of f~2-3 climate gain due to the fast feedback processes. This same f should apply to the climate gain due to greenhouse-gas radiative heating. Taking into account of the uncertainties, the range of f is $1.7<f<4.7$. The range of global warming at equilibrium due to doubling CO_2 is $1.4f$ °K, or between 2.3 and 6.4 °K. The lower bound is relatively firm, while the “upper bound” is more uncertain due to the form and value of heat flux assumed. Since it is also higher than the upper bound of Foster and Gregory, the latter’s upper bound is adopted instead. Therefore the uncertainty in our treatment of ocean uptake does not enter into our final result (2), but the exercise serves to demonstrate the feasibility of a TSI explanation of the cause of the solar-cycle warming at the surface.

FIGURE LEGENDS

Figure 1. Annual-mean, global-mean NCEP surface air temperature (1959–2004), in red, with scale on the left axis. The blue line shows the annual-mean TSI time series [*Lean, et al.*, 1995], updated and provided to us by Dr. J. Lean, with scale on the right axis. κ is the regression of global-mean temperature response in °K per each Wm^{-2} variation of the solar constant. ρ is the correlation coefficient between the global temperature and the TSI. An isospectral Monte-Carlo test, in which the spectral phase of the temperature (or the TSI) time series is randomized while preserving the spectral amplitude to generate 3,000 synthetic time series, shows that this positive value of ρ is not likely to occur by chance.

Figure 2. Surface temperature from NCEP 1959-2004. (a) The coherent latitudinal pattern which best distinguishes the years in the solar-max group (when TSI is 0.06 Wm^{-2} above the mean) from the years in the solar-min group (when TSI is 0.06 below the mean), normalized so that its global mean is one. (b) Bootstrap with replacement Monte-Carlo test, showing that the separation *R* achieved by the pattern in (a), indicated by the vertical blue line, is not likely to be achieved by 10,000 time series generated by randomly assigning, with replacement, the same number of years to the solar-max/min group as in the real data. (c) LDA filtered (projected) time series of temperature data. This projection is scaled such that the left axis shows the global-mean temperature anomaly. To obtain the temperature anomaly at a particular latitude, multiple (a) into (c). The red pluses are temperatures in the solar-max group and the blue circles are in the solar-min group. The black line shows the annual-mean TSI time series with scale on the right axis. The small solid circles indicate the years used in the analysis, while the hollow small circles indicate the years dropped. These are the years of the volcanoes discussed in the text, and the years when the TSI variability is close to its mean, which are considered to be neither solar max nor solar min. Prior to the LDA analysis, NCEP time series at different latitudes are detrended and regularized (smoothed in space) using truncated SVD decomposition, at truncation level r=17 , chosen as discussed in *Camp and Tung* [2007a]

Figure 3. Same as in Figure 1, except for the mean temperature in the 850-500 hPa layer. Because the topography of the Antarctic continent protrudes into this layer even in zonal mean, the region 70^o S-90^oS is excluded. This exclusion affects the global-mean temperature only minimally because of the small polar area.

Figure 4. The global surface pattern of temperature that best distinguishes the solar-max group from the solar-min group. Shown in color is the temperature difference in °K between ± one standard deviation from the mean. The actual peak-to-peak difference between the solar max and solar min is larger, but not as robust as the standard-deviation difference. A measure of the peak-to-peak difference can be obtained by multiplying the values shown by a factor of $\pi/2$. Monte-Carlo test shows that this global pattern is statistically significant above the 95% confidence level.

Figure 5: Same as Figure 4, except in polar stereographic projection centered on the North Pole (left) and on the South Pole (right).

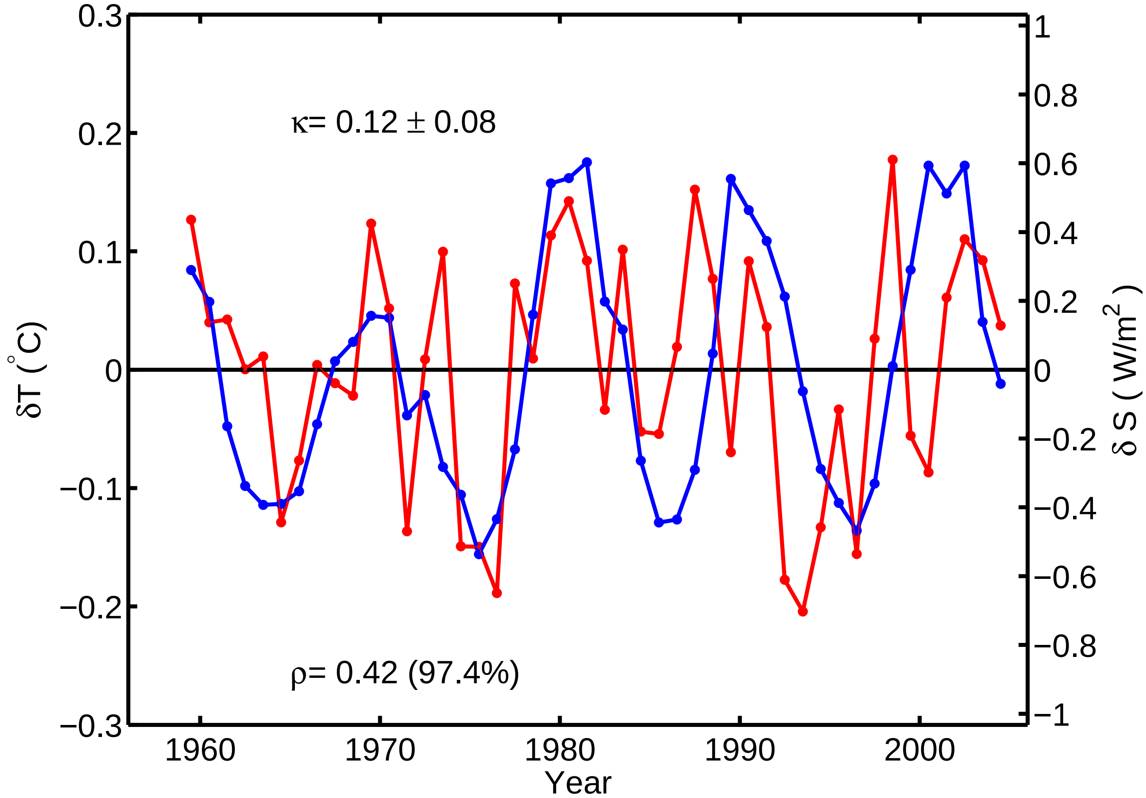

Figure 1. Annual-mean, global-mean NCEP surface air temperature (1959–2004), in red, with scale on the left axis. The blue line shows the annual-mean TSI time series [*Lean, et al.*, 1995], updated and provided to us by Dr. J. Lean, with scale on the right axis. κ is the regression of global-mean temperature response in °K per each Wm^{-2} variation of the solar constant. ρ is the correlation coefficient between the global temperature and the TSI. An isospectral Monte-Carlo test, in which the spectral phase of the temperature (or the TSI) time series is randomized while preserving the spectral amplitude to generate 3,000 synthetic time series, shows that this positive value of ρ is not likely to occur by chance.

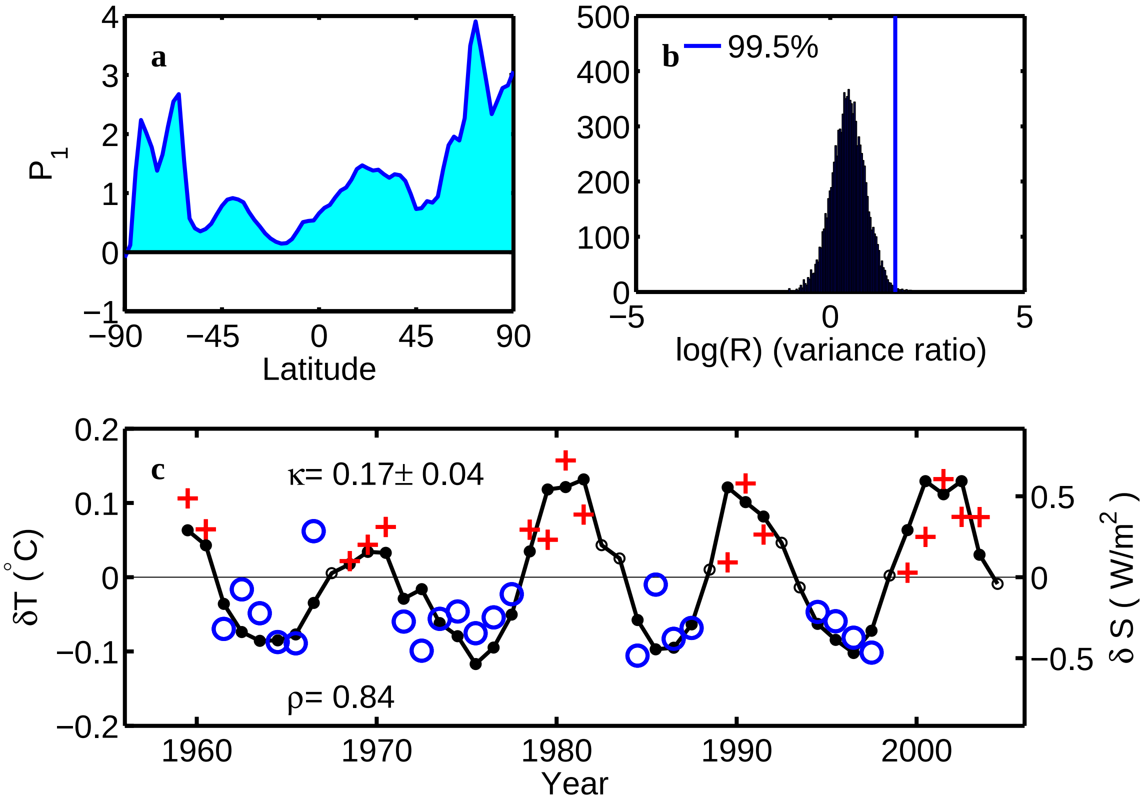

Figure 2. Surface temperature from NCEP 1959-2004. (a) The coherent latitudinal pattern which best distinguishes the years in the solar-max group (when TSI is 0.06 Wm^{-2} above the mean) from the years in the solar-min group (when TSI is 0.06 below the mean), normalized so that its global mean is one. (b) Bootstrap with replacement Monte-Carlo test, showing that the separation *R* achieved by the pattern in (a), indicated by the vertical blue line, is not likely to be achieved by 10,000 time series generated by randomly assigning, with replacement, the same number of years to the solar-max/min group as in the real data. (c) LDA filtered (projected) time series of temperature data. This projection is scaled such that the left axis shows the global mean temperature anomaly. To obtain the temperature anomaly at a particular latitude, multiple (a) into (c). The red pluses are temperatures in the solar-max group and the blue circles are in the solar-min group. The black line shows the annual-mean TSI time series with scale on the right axis. The small solid circles indicate the years used in the analysis, while the hollow small circles indicate the years dropped. These are the years of the volcanoes discussed in the text, and the years when the TSI variability is close to its mean, which are considered to be neither solar max nor solar min. Prior to the LDA analysis, NCEP time series at different latitudes are detrended and regularized (smoothed in space) using truncated SVD decomposition, at truncation level r=17 , chosen as discussed in [*Camp and Tung*, 2007a]

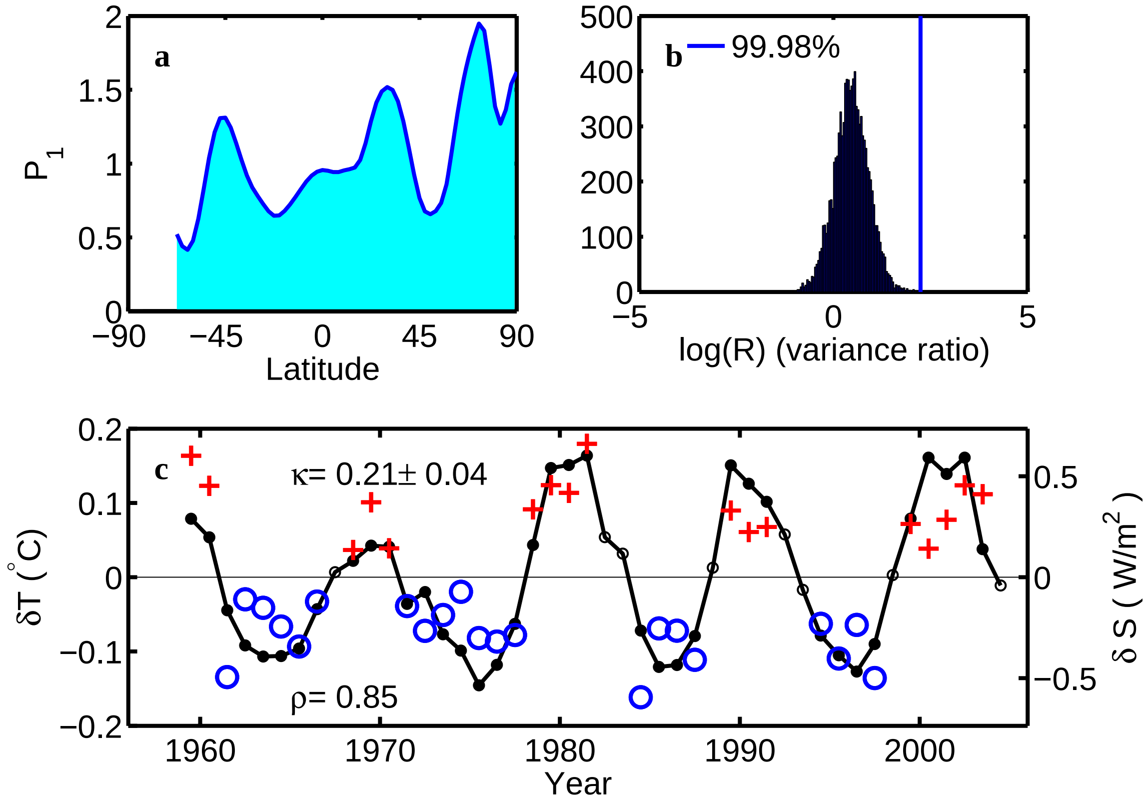

Figure 3. Same as in Figure 1, except for the mean temperature in the 850-500 hPa layer. Because the topography of the Antarctic continent protrudes into this layer even in zonal mean, the region 70° S-90°S is excluded. This exclusion affects the global mean temperature only minimally because of the small polar area.

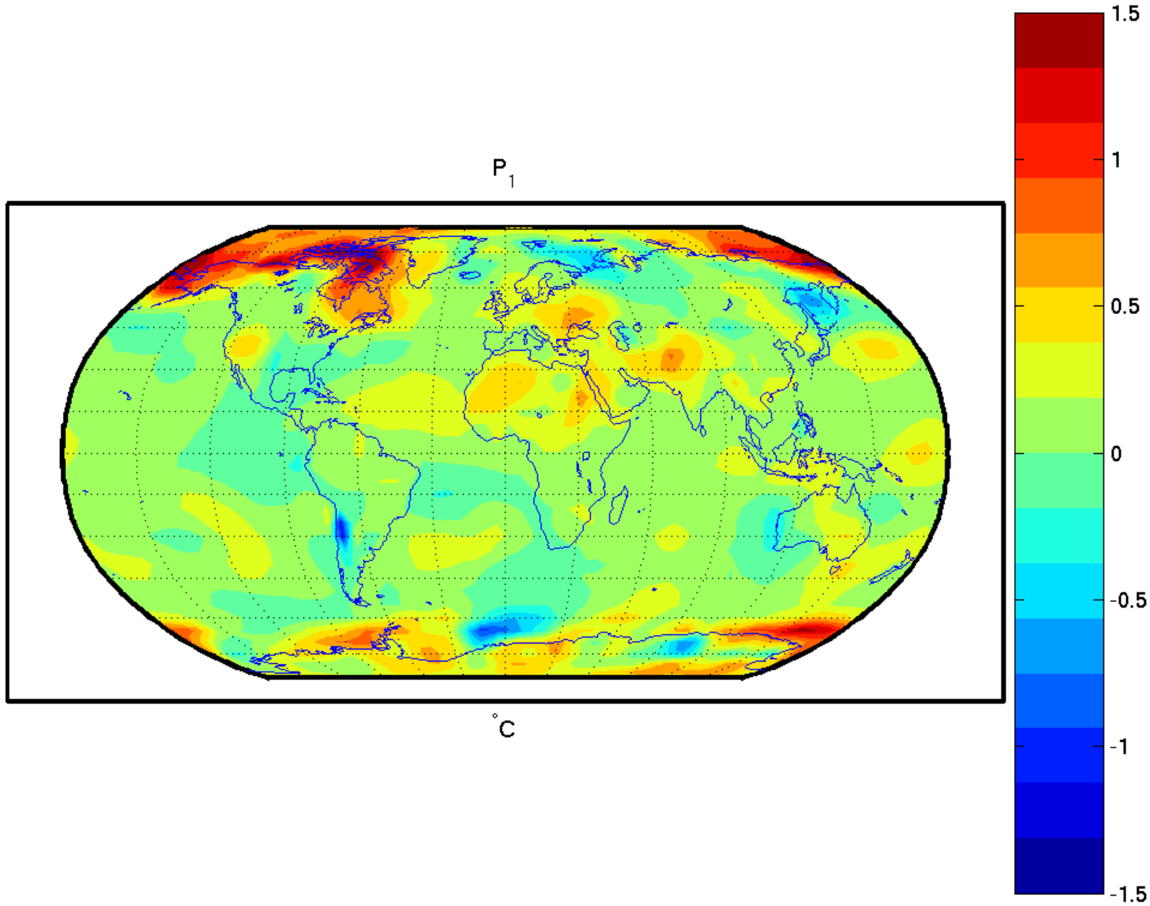

Figure 4. The global surface pattern of temperature that best distinguishes the solar-max group from the solar-min group. Shown in color is the temperature difference in °K between ± one standard deviation from the mean. The actual peak-to-peak difference between the solar max and solar min is larger, but not as robust as the standard-deviation difference. A measure of the peak-to-peak difference can be obtained by multiplying the values shown by a factor of $\pi/2$. Monte-Carlo test shows that this global pattern is statistically significant above the 95% confidence level.

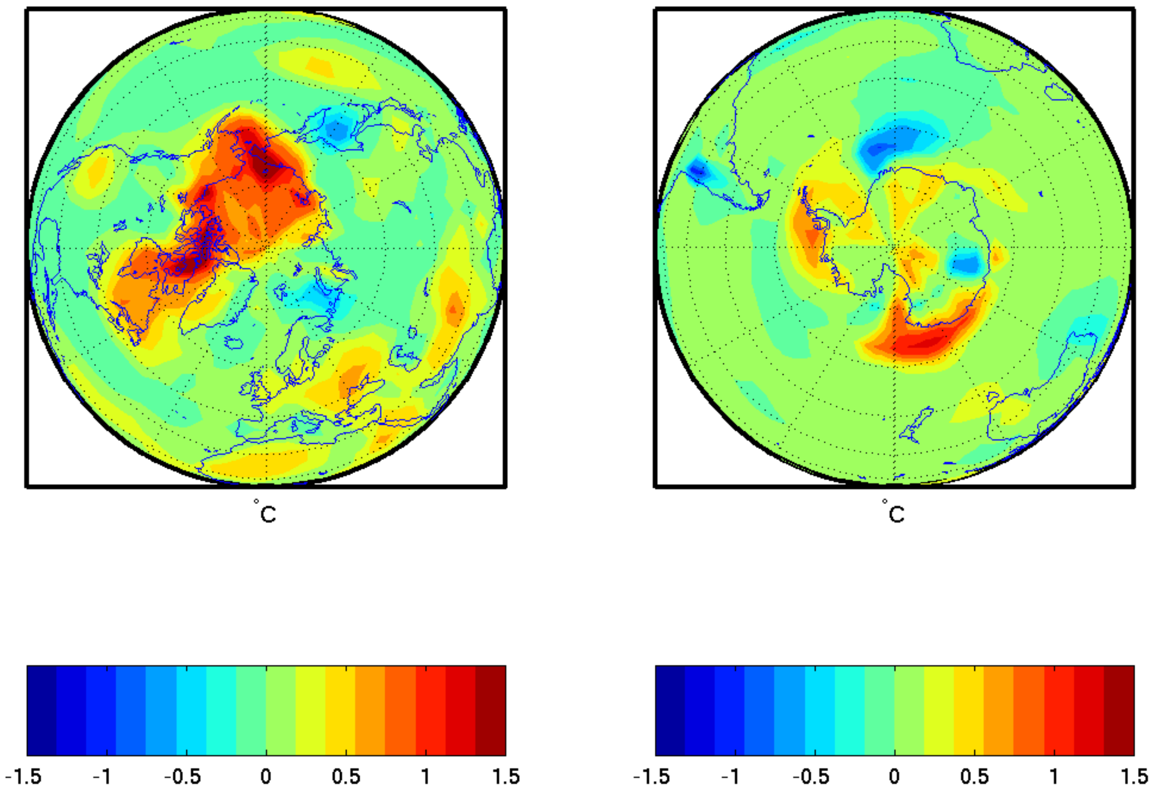

Figure 5: Same as Figure 4, except in polar stereographic projection centered on the North Pole (left) and on the South Pole (right).